Proceedings of the 12th International Conference on
Aluminium Alloys, September 5-9, 2010, Yokohama, Japan

pp. 1243-1248

Mechanical and Forming Properties of AA6xxx Sheet from Room to Warm Temperatures

Alexis Miroux[1], Manojit Ghosh[1,2], Srihari Kurukuri[1,3], Leo Kestens[2] and Ton van den Boogaard[3]

[1]Materials innovation institute (M2i), Mekelweg 2, 2628 CD Delft, the Netherlands

[2]Materials Science and Engineering department, Delft University of Technology, Mekelweg 2, 2628 CD Delft, the Netherlands

[3]Faculty of Engineering Technology, University of Twente, P.O. box 217, 7500 AE Enschede, the Netherlands

The influence of temperature on the mechanical behaviour of the heat treatable Aluminium alloy EN AW-6061 has been investigated with a series of tensile tests. It is found that temperature has an effect on both the storage of dislocations and dynamic recovery. The results have been used to fit the dislocation based Nes work-hardening model. Simulations show that the model captures properly the dependence of yield stress and work-hardening rate with temperature and temper. The work-hardening model has been implemented into the Dieka FEM to simulate the warm deep drawing of cylindrical cups. Comparison of the simulated and experimental punch force and cup thickness reveals a good correspondence and validates the proposed modelling approach.

Keywords: *forming, temperature, work-hardening, tensile, FEM.*

1. Introduction

Finite element modelling is nowadays a common numerical technique to simulate sheet metal forming operation. The material behaviour required as an input of the model can be obtained from experimental measurement of from the coupling with a material model. Such coupling have been implemented for room temperature forming but still need to be developed for the case of warm forming. This particular forming process is regarded as a promising way for increasing the relatively low formability Aluminium alloys. This paper presents the application of the work-hardening model developed by Nes [1] to the simulation of the behaviour of 6xxx Aluminium alloys as a function of temperature and its implementation to the Dieka FEM model [2]. Deep drawing of cylindrical cups is used to illustrate the performance of the coupled models.

2. Tensile test experiment

Aluminium alloy EN AW-6061 in the form of rolled sheet has been used for the present investigation. The sheet has been cold rolled, solution treated, quenched and naturally aged (T4). The thickness of the sheet was 1.21 mm. The alloy contains 0.62 Si, 0.35 Fe, 0.2 Cu, 0.08 Mn, 0.95 Mg, 0.15 Cr and other elements below 0.15 wt%. Naturally aged material has been converted to peak aged condition or T6 by applying a heat treatment, at 150°C for 4 hours followed by 170°C for 4 hours in salt bath and quenching in water.

Tensile tests were carried out at room temperature (RT) and 250°C with the thermo-mechanical simulator Gleeble 1500. Specimens were heated by Joule effect and the deformation was measured with an extensometer attached at the middle of the specimen, starting with a gauge length of 10 mm. The tensile direction was the rolling direction and the strain rate was 0.01 s^{-1}.

Fig. 1 shows the stress-strain curves and Fig. 2 the work-hardening rate curves for the two tempers at both temperatures. The Voce equation has been fitted on the stage III part of the curves in order to determine the initial work-hardening rate ($\theta_0 = \frac{d\sigma}{d\varepsilon_p}$ at beginning of stage III) and dynamic recovery parameter ($\beta = \frac{d\theta}{d\sigma}$ during stage III)(Table1).

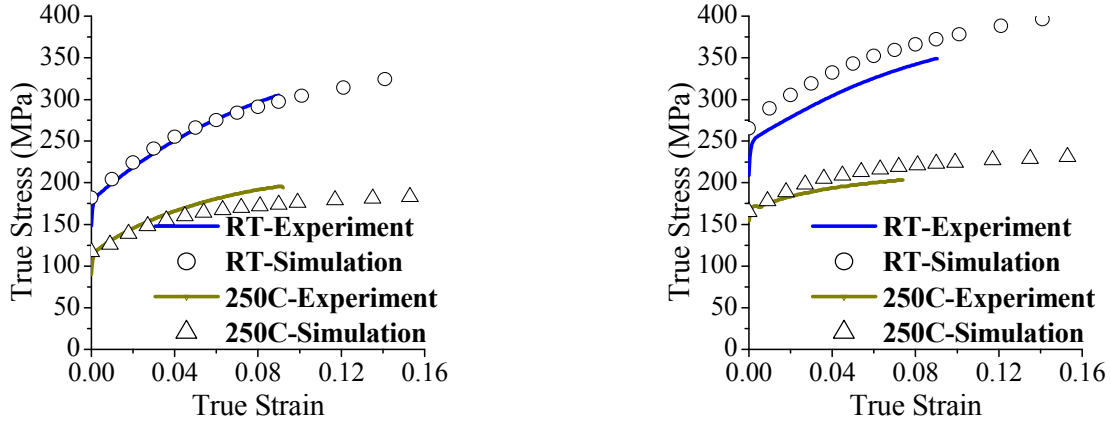

Fig. 1. Experimental (tensile test) and simulated (Nes model) true stress-true strain curves of (a) 6061-T4 and (b) 6061-T6 sheets at room temperature and 250°C

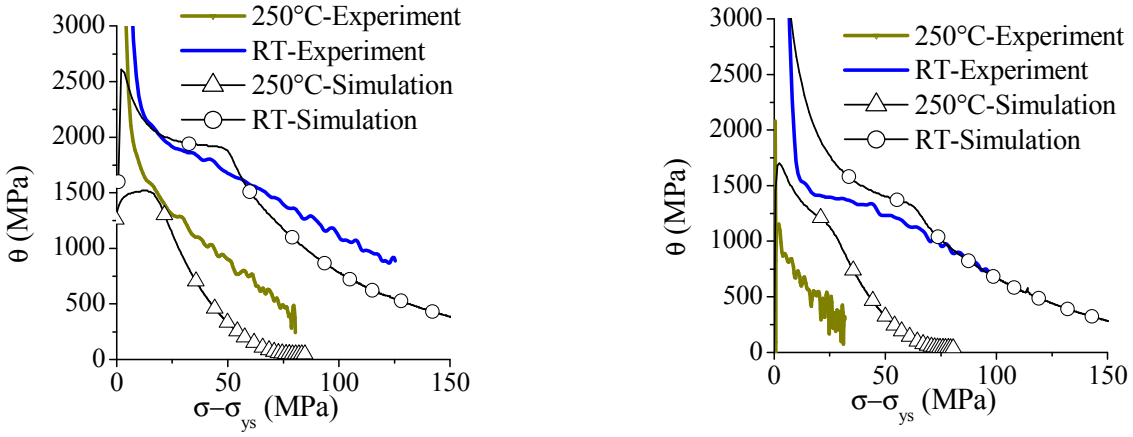

Fig. 2. Experimental (tensile test) and simulated (Nes model) work-hardening rate of (a) 6061-T4 and (b) 6061-T6 sheets at room temperature and 250°C

Table 1. Yield stress and parameters of the Voce equation fitted to the experimental tensile test results

	T4 – RT	T4 – 250°C	T6 – RT	T6 – 250°C
$YS_{0.2\%}$ (MPa)	178	115	247	171
θ_0 (MPa)	2200	1880	1630	970
$\lvert\beta\rvert$	10.8	19.2	9.5	23.1

As expected, the T6 material shows higher yield stress and lower work-hardening rate at both temperatures compared to the T4 one. The higher yield stress of T6 is usually related to larger, hence stronger, precipitates. The lower work-hardening rate of T6 comes from a lower value of θ_0. The low value of θ_0 indicates that, as for the T4 material, precipitates in T6 condition are not efficient in storing dislocations and that dislocation storage during the underaged regime is mainly controlled by the solute content [3, 4]. The β parameter values of both tempers are very close. The values at room temperature are similar to the one reported for AA6111 [5] or for AA6005A [4], meaning that dynamic recovery in AA6xxx series is relatively independent of the exact solute content and precipitate distribution. As already reported in literature, e.g. [6], the yield stress and the work-hardening rate decrease when the deformation temperature increases. The decreases of work-hardening rate is related to a decrease of dislocation obstacle efficiency (decrease of θ_0) and to the thermal activation of dynamic recovery (increase of $|\beta|$).

3. Work-hardening model

To predict the material behaviour accurately by FEM it is necessary to combine it with a material model, which simulates the strength and work-hardening response of the material. The dislocation based work-hardening model developed by Nes [1, 7-9] was selected for the present research. The main objective of this model is to develop a unified theory of deformation that can predict the stress-strain behaviour for fcc metals or alloys under any level of strain rate and temperature. This model was already applied to the simulation of the work-hardening of 6xxx Aluminium alloys at room temperature [10].

For the present work version V201 of the model was used and the code was received from the group of E. Nes at NTNU, Norway. The original equation for the contribution of dispersoids to the flow stress has been replaced by an equation more suitable for the smaller precipitates present in heat treatable alloys [10, 11]:

$$\sigma_p = M\left(\frac{3f}{2\pi}\right)^{\frac{1}{2}} 2\beta^* G\frac{b}{r}\min\left(\frac{r}{r_c},1\right)^{\frac{3}{2}}, \tag{1}$$

where M is the Taylor factor, G the shear modulus, b the Burgers vector, β^* a constant related to the dislocation line tension, f the volume fraction and r the average radius of the precipitates, and r_c the transition radius between particle shearing and by-passing mechanisms.

The Nes model uses a statistical treatment to calculate the mean slip length of the dislocation. The contribution of precipitates to the mean slip length is given by

$$L_p = \frac{1}{\kappa_3}\frac{r}{2f}, \tag{2}$$

with κ_3 a constant. In AA6xxx, small precipitates (with $r < r_c$) can be sheared and consequently do not contribute to the slip length [4, 5, 12]. Assuming that precipitate sizes are distributed according to a log-normal distribution, only those precipitates with $r > r_c$ will contribute to dislocation storage. Furthermore, by-pass of non-shearable precipitates, as the ones present in T6 condition, by dislocation leaves Orowan loops around the precipitates. Experimental results, however, show that the initial WH rate (θ_0) of T6 or peak-aged materials is minimum meaning the precipitates are not efficient in storing dislocations. Following the treatment of Simar [4], it is assumed that Orowan loops can still shear a precipitate if its size is smaller than the size of fully incoherent precipitates. An efficiency factor (φ) was defined as the proportion of Orowan loops that don't annihilate by shearing. It is assumed that the dislocation density increment due to precipitates, which is proportional to κ_3,

also scales with the proportion of Orowan loops that remain. The κ_3 parameter is then modified according to

$$\kappa_3 = \kappa_{3p}\varphi\left(\bar{r}_c\right)\frac{r}{r_c}\frac{f_c}{f}, \tag{3}$$

with $\bar{r}_c$ the mean radius and f_c the volume fraction of the precipitates with $r > r_c$, and κ_{3p} the parameter defined in the initial version of the model.

4. Simulations and discussion

The grain size of T4 (16 μm) and T6 (15 μm) materials have been measured on micrographs and the Taylor factor (3) has been calculated from the textures measured by XRD. The initial dislocation density is taken as 10^{11} m^{-2}. Precipitates in the T4 material are assumed to be GP zones with the stoichiometry $Al_9Mg_2Si_1$ [13] and precipitates in the T6 material are supposed to be β" with the stoichiometry Mg_5Si_6 [14]. Precipitate average size (r), number density (N), and volume fraction (f) were determined using existing data in literature and by fitting the yield stress calculated with the model of Myhr [11] to the experimental data at room temperature. The solute contents were obtained from the mass balance.

Four parameters have been adjusted to fit the Nes model to the experimental stress-strain curves simultaneously for two alloys, 6061 and 6016 (not shown here), two tempers, T4 and T6, and at two temperatures, 20ºC (room temperature) and 250ºC. All other parameters have been taken from literature. First the concentration exponent in the activation volume used for the thermal stress expression is obtained by fitting the yield stress at room temperature (e_t = 0.58). The temperature dependence of the yield stress is fitted by making the transition radius, r_c, dependent on temperature, with a value of 5 nm at room temperature and 6.4 nm at 250ºC. The dislocation storage parameter, C, and the scaling parameter, q_c, are obtained by fitting the work-hardening rate. These parameters are assumed independent of temperature but are fitted separately for T4 (C = 30 and q_c = 9) and T6 (C = 50 and q_c = 7) materials. The simulated stress-strain curves and work-hardening rate curves are plotted in Fig. 1 and Fig. 2 respectively.

From Fig. 1, it can be seen that the model reproduces correctly the dependence of yield stress with temperature and temper, although some quantitative differences may remain as for the T6 temper at room temperature. In the literature, the depletion of solutes during ageing is considered to be responsible for the experimentally observed decrease of initial work-hardening rate [3, 4]; solute depletion results in an increase of the mean free path, which is translated in the Nes model by an increase of the C parameter. The higher fitted C value for T6 condition compared to T4 reflects this effect of solutes. The scaling parameter, q_c, relates the dislocation cell size with the dislocation density inside the cells. The continuous decrease of the fitted q_c values when going from 5xxx [7] to 6061-T4 and to 6061- T6 shows that increasing the amount of precipitates and/or decreasing the amount of solutes promotes the formation of cell walls at the expense of the storage of dislocation inside the cells. This results in an increase of the work-hardening rate in stage III, partially balancing the effect of C. The model reproduces qualitatively the decrease of work-hardening rate with increasing temperature from 20°C to 250°C for both tempers (Fig. 2). However, experimental measurements show that the difference of work-hardening rate between T4 and T6 tempers increases with temperature while the modelled work-hardening rates converge. The reason for this difference still needs to be further investigated.

5. Application to deep drawing

In this section, application of the presented model for the finite element simulation of warm deep drawing of cylindrical cups made of 6061 is presented. A temperature and strain rate dependent

anisotropic material model for finite element analysis was implemented into the in-house implicit finite element code DiekA. Implementation details are given elsewhere [2]. The anisotropic behaviour of the sheet is described by using the Vegter yield function [15], which is purely based on experimental measurements.

Orthotropic symmetry was assumed for the material model. A quarter of the blank was modelled and boundary conditions were applied on the displacement degrees of freedom to represent the symmetry. The sheets were modelled with 2820 discrete Kirchhoff triangular shell elements with 3 translational, 3 rotational and 1 temperature degree of freedom per node. The tools were modelled as rigid contours with a prescribed temperature. In the presented simulations room temperature deep drawing was simulated by giving a temperature of 25°C to the punch, the die, and the blank holder. For warm deep drawing, the die and the blank holder were given a temperature 250°C, while the punch was kept at 25°C. In the simulations, the friction between the sheet and rigid tools (die and cheeks) is described with Coulomb's friction model with a friction coefficient of 0.06 for room temperature simulations and 0.12 for warm forming conditions. During experimental deep drawing, the force-displacement curve of the punch was recorded. After the experiments, the cups were removed and the thickness distribution from the centre to the outer diameter in the rolling direction was measured (with an accuracy of ± 0.012 mm). The force-displacement curve and the thickness data are used to validate the simulations.

Comparing the different punch force–displacement curves (Fig. 3), it can be seen that the model performs very well at all the temperatures. At 25°C, the simulated maximum punch force is in good agreement with the experiments and the punch force is underestimated at larger drawing depths. The maximum punch force at 250°C is slightly shifted from the experiments.

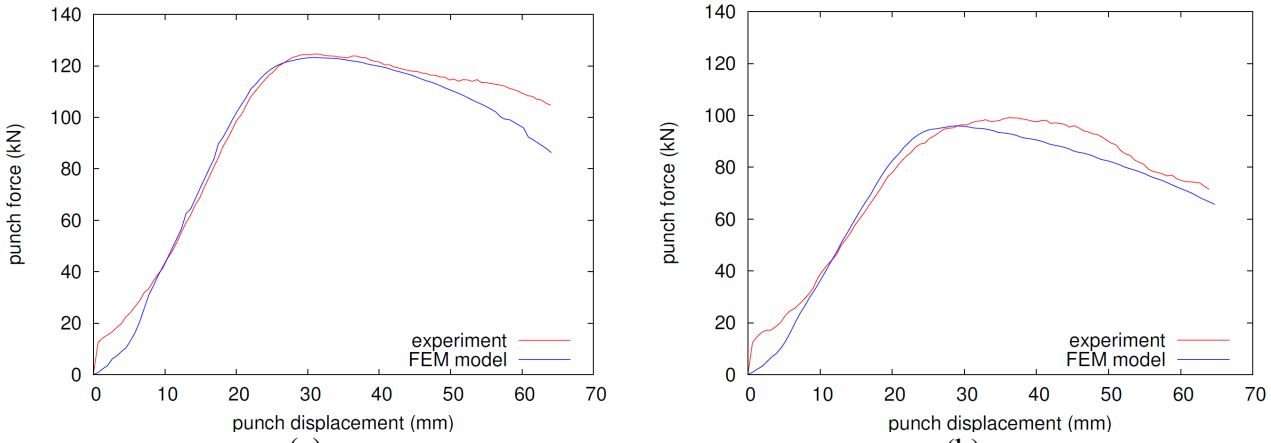

Fig. 3. Punch force–displacement curves for AA 6061-T4 alloy for (a) room temperature deep drawing (25°C) and (b) warm deep drawing (250°C)

Experimental measurements in Fig. 4 show that the bottom (part of the curve from 0 to 45 mm) is thiner after room temperature drawing than after warm drawing. The reason is that during warm drawing, the flange is warmer and therefore softer than the bottom and carries relatively more deformation than in case of room temperature drawing. The FEM model, however, predicts the same thickness at the bottom at both drawing temperatures. FEM simulations also show that the trends along the wall (curve from 45 to 120 mm) and flange (curve above 120 mm) with changing temperature are well predicted (Fig. 4).

It can therefore be conclude that the combination of the physically based material model of Nes with the finite element code DiekA and a proper description of the plastic anisotropy gives good predictions of the forming process at various temperatures. This model combination offers the possibility to explore the effect of material and process parameters without the need of additional fitting.

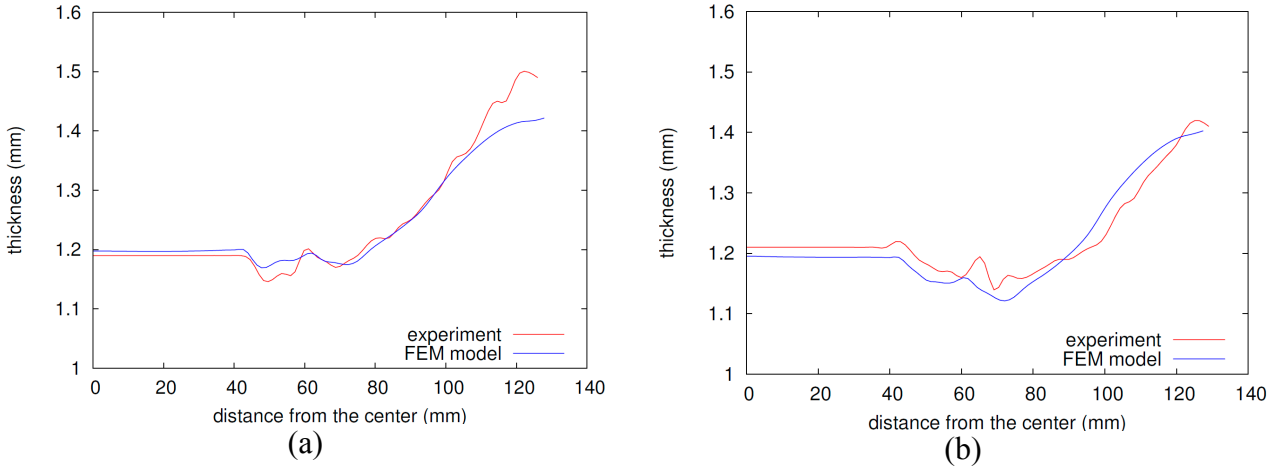

Fig. 4. Thickness distribution curves for AA 6061-T4 alloy for (a) room temperature deep drawing (25°C) and (b) warm deep drawing (250°C)

Acknowledgement

This research was carried out under the project number MC1.02106 in the framework of the Research Program of the Materials innovation institute M2i (www.m2i.nl). All the partners of the project are highly acknowledged for their collaboration and support. The authors also gratefully thank B. Holmedal at NTNU for giving us the permission to use the code of the Nes model for this research.

References

[1] E. Nes: Progress in Materials Science 41 (1998) 129-193
[2] S. Kurukuri, A. H. van den Boogaard, A. Miroux and B. Holmedal: Journal of Materials Processing Technology 209 (2009) 5636–5645.
[3] D.J. Lloyd: Materials Science Forum 519-521 (2006) 55-61
[4] A. Simar, Y. Bréchet, B. de Meester, A. Denquin and T. Pardoen: Acta Materialia 55 (2007) 6133-6143
[5] L.M. Cheng, W.J. Poole, J.D. Embury and D.J. Lloyd: Metallurgical and Materials Transactions 34A (2003) 2473-2481
[6] D. Li and A. Ghosh: Materials Science Engineering A352 (2003) 279-286
[7] K. Marthinsen and E. Nes: Materials Science and Technology 17 (2001) 376-388
[8] E. Nes and K. Marthinsen: Materials Science Engineering A322 (2002) 176-193
[9] B. Holmedal, K. Marthinsen and E. Nes: Z. Metallkunde 96 (2005) 532-544
[10] J. Friis, B. Holmedal, Ø. Ryen, E. Nes, O.R. Myhr, Ø. Grong, T. Furu and K. Marthinsen: Materials Science Forum 519-521 (2006) 1901-1906
[11] O.R. Myhr, Ø. Grong and S.J.Andersen: Acta Materialia 49 (2001) 65-75
[12] W.J. Poole and D.J. Lloyd: Proceedings of the 9th International Conference on Aluminium Alloys, Ed. J.F. Nie, A.J. Morton and B.C. Muddle, (Institute of Materials Engineering Australasia Ldt, 2004) pp. 939-944
[13] M. Murayama and K. Hono: Acta Materialia 47 (1999) 1537-1548
[14] J.H. Chen, E. Costan, M.A.van Huis, Q. Xu and H.W. Zandbergen: Science 312 (2006) 416-419
[15] H. Vegter and A. H. van den Boogaard: International Journal of Plasticity 22 (2006) 557–580.